Journal of
Polymer Materials

Tech Science Press

http://doi.org/10.32604/jpm.2026.081663

ARTICLE

Schisandra Lignans- and MSCs-Laden Microgels Attenuate Inflammation on LPS-Induced HepG2 Cells in a PEGNB Hydrogel Model

Xingdan Wang[1,#], Lei Yang[1,#], Renmeng Liu[1], Yuheng Du[1], Zhihuan Li[1], Xinyue Zhang[1], Linhao Zhu[1] and Ni Ren[2,*]

[1]Department of Chemical Engineering, University of Science and Technology Liaoning, Anshan, China
[2]Department of Applied Technology, University of Science and Technology Liaoning, Anshan, China
*Corresponding Author: Ni Ren. Email: netc_renni@163.com
#These authors contributed equality to this work

Received: 06 March 2026; Accepted: 25 June 2026; Published: 24 September 2026

ABSTRACT: Hepatitis has imposed a substantial burden on human health. Tumor necrosis factor-α (TNF-α) drives the inflammatory response by triggering downstream signaling, particularly the nuclear factor kappa B (NF-κB) pathway. Suppressing NF-κB activation represents a promising therapeutic strategy. PEGNB, a polymeric hydrogel, exhibits significant potential due to its superior cytocompatibility. We developed a controlled-delivery microgel platform by encapsulating Schisandra lignans (SLs) and mesenchymal stromal cells (MSCs) in polyethylene glycol-norbornene (PEGNB) microgels. To mimic an inflammatory hepatic microenvironment *in vitro*, Lipopolysaccharide (LPS)-induced HepG2 cells were encapsulated in bulk PEGNB hydrogel. The microgel–cell system enabled localized co-delivery of SLs and MSCs paracrine factors to LPS-induced cell-laden hydrogel constructs. SLs were extracted from *Schisandra chinensis* raw powder, yielding 0.83 mg/g of deoxyschisandrin and 2.51 mg/g of schisandrin. Based on the MTT assay, concentrations ≤ 5.6 μM were selected as a non-cytotoxic working range for subsequent *in vitro* studies. Microfluidic technology was used to fabricate PEGNB microgels with high monodispersity and diameters ranging from 130–170 μm. PEGNB-based microgels enabled the co-delivery of SLs and MSCs, serving as a polymeric platform for attenuating hepatic inflammatory responses while maintaining high cell viability above 70% and achieving sustained SLs release of 82.31 ± 4.35% over 14 days. In this model, SLs–MSC-laden microgels significantly reduced TNF-α and Interleukin-6 (IL-6) expression compared with untreated controls, and the combined SLs–MSC treatment produced a greater reduction than either SLs or MSCs alone. These results support PEGNB-based microgel co-delivery of SLs and MSCs as a promising strategy to attenuate inflammatory responses in an *in vitro* hepatic inflammation model.

KEYWORDS: PEGNB hydrogel; mesenchymal stromal cells; microfluidics; hepatitis; anti-inflammation

1 Introduction

Hepatitis can be classified into acute and chronic types, which imposes a profound global health challenge [1,2]. Acute hepatitis results from viral infections or drug-induced liver injury [3]. Chronic hepatitis is characterized by persistent inflammation. This chronic state frequently drives progressive fibrosis and cirrhosis [4]. It significantly elevates the risk of hepatocellular carcinoma [5,6]. TNF-α, a pleiotropic cytokine during hepatitis, plays a central role in the inflammatory response [7]. Elevated TNF-α levels are closely associated with disease activity in both acute and chronic liver inflammation. During inflammation, TNF-α binds to its receptors, TNFR1 and TNFR2, activating downstream signaling pathways, notably the NF-κB signaling pathway [8]. NF-κB activation induces the transcription of proinflammatory genes like

Interleukin-1β (IL-1β) and IL-6. These factors amplify and sustain inflammatory responses [9]. NF-κB triggers anti-apoptotic genes such as B-cell lymphoma-extra large and X-linked inhibitor of apoptosis protein. These genes promote hepatocyte survival under inflammatory stress [10]. Regulating the TNF-α-mediated NF-κB signaling axis represents a promising strategy to attenuate hepatic inflammation [11]. Compounds modulating this pathway may serve as candidates for treating hepatitis-associated conditions [12].

The traditional medicinal herb *Schisandra chinensis* has been used for centuries to alleviate fatigue and exert hepatoprotective effects [13]. Advances in extraction methods have facilitated extensive research on SLs. Key constituents include deoxyschisandrin, schisandrin A, and schisandrin C. The anti-inflammatory activity of *Schisandra chinensis* lignans has been associated with structural features such as methoxy and methylenedioxy groups [14]. As deoxyschisandrin and schisandrin are major and widely studied Schisandra lignans, they were selected as representative SLs markers in this study. Previous work has demonstrated that SLs possess anti-inflammatory potential for hepatitis by modulating the NF-κB signaling pathway [15]. It has been demonstrated that schisandrin has the potential to ameliorate the inflammatory microenvironment by downregulating inducible nitric oxide synthase and cyclooxygenase-2 [16]. This may create a microenvironment that is suitable for cell survival. Another study has shown that *Schisandra chinensis* lignans suppress LPS-induced inflammatory responses by reducing the phosphorylation of IKKα/β, IκBα, and NF-κB p65 and inhibiting NF-κB p65 nuclear translocation [17]. These findings suggest that SLs are promising candidates for hepatitis therapy. A single large dose of SLs induces cytotoxicity in hepatocytes [18], limiting their direct application. A delivery strategy that enables sustained and localized release of SLs is critical to maximize their therapeutic efficacy while minimizing adverse cellular effects [19].

Several studies have shown that MSCs exert broad therapeutic effects in hepatitis, including immunomodulation [20], anti-apoptotic activity [21] and tissue regeneration [22]. It is generally believed that MSCs inhibit the activation of inflammatory signaling pathways primarily via a paracrine mechanism rather than directly interacting with target cells. Within co-culture systems *in vitro*, MSCs are sensitive to their surrounding inflammatory microenvironment and the paracrine activity of MSCs is associated with the microenvironment, as excessive cytokines impair the survival and paracrine activity of MSCs [23,24]. When MSCs are not encapsulated, exposure to high levels of inflammatory cytokines can impair their survival [25], paracrine function, and even lead to cytotoxicity. Modulation of the inflammatory microenvironment is particularly important for MSC-based co-culture systems. In the inflammatory environment, the anti-inflammatory cytokine IL-10 is released by MSCs and inhibits the NF-κB signaling pathway, leading to the attenuation of TNF-α and IL-6 gene expression in inflammatory cells [26]. MSCs have been shown to inhibit LPS-induced NF-κB activation by reducing IKKβ, p-IκBα, p-IκBβ, and nuclear p65 levels [27]. Given these challenges, it is crucial to develop a delivery system that protects MSCs from the harsh inflammatory environment while preserving their therapeutic effects.

Taken together, the above evidence suggests that both SLs and MSCs may contribute to inflammatory regulation through complementary mechanisms. These findings provide a literature basis for discussing the possible involvement of NF-κB-related signaling in our SLs-MSC co-delivery system.

PEGNB hydrogels are formed through a rapid and well-controlled photoinitiated thiol-norbornene crosslinking process under mild light exposure [28], offering excellent spatiotemporal control over gelation [29]. As they are transparent [30] and provide a highly cytocompatible microenvironment resembling *in vivo* [31,32], the hydrogels excel at cell encapsulation, enabling long-term monitoring and maintenance of cellular behavior. The tunable physical and biochemical characters make the hydrogels advantageous for simulating the dynamic *in vivo* microenvironment [33,34]. PEGNB hydrogels are suitable for cell encapsulation and support high cell viability [35,36]. PEGNB microgels embedded within a bulk hydrogel enable

spatial compartmentalization of MSCs and SLs, allowing regulated paracrine and diffusional crosstalk with co-encapsulated HepG2 cells [37]. A previous study has shown that MSCs encapsulated in PEGNB microgels maintain high cell viability [38]. As a drug delivery platform, PEGNB microgels exhibit great transport properties. The diffusion rate of SLs and MSC-derived cytokines was facilitated, due to the hydrogels' semipermeability [39] and high water content [40]. The release of bioactive molecules can be precisely regulated by adjusting the crosslinking degree, as the pore size of PEGNB networks conversely decreases with crosslinking density [41].

This study focuses on developing a PEGNB hydrogel model that encapsulates LPS-induced HepG2 cells to simulate an inflammatory liver microenvironment, along with SLs-MSC-laden PEGNB microgels. The aim is to evaluate the combined anti-inflammatory effects for hepatitis [12]. This system is designed to assess the reduction of pro-inflammatory cytokines such as TNF-α and IL-6 and the sustained release of SLs and MSCs-derived cytokines. This strategy provides a promising approach for an integrated drug-cell delivery platform for treating hepatitis.

2 Materials and Methods

2.1 Preparation of Schisandra Lignan Extract

The dried *Schisandra chinensis* fruits were ground into powder and soaked in 95% ethanol for 2 h to pre-washing. The soaked powder was dried in an oven at 60°C for 12 h. Then, 10 g of the dried powder was extracted with 100 mL ethanol under reflux for 1.5 h. The mixture was filtered under vacuum through a 0.22 μm membrane filter. The filtrate was stored at −20°C for more than 24 h, and the lignans in the solution were quantified by GC-MS. The solvent was evaporated by drying the solution in an oven at 60°C for 16 h. The resulting dried extract was dissolved in PBS to prepare the stock solution.

2.2 Cell Culture

HepG2 cells were maintained in low glucose Dulbecco's modified Eagle's medium (DMEM; Biosharp, CHN), supplemented 10% fetal bovine serum (FBS; Biosharp, CHN), 1% antibiotic-antimycotic (Biosharp, CHN). Cells were incubated at 37°C under an atmosphere with 5% CO_2. The culture medium was refreshed once every two days and cells were subculture with 0.05% trypsin when they reached approximately 70–80% confluence. Mouse MSCs were cultured in low glucose Dulbecco's modified Eagle's medium (DMEM; Biosharp, CHN), supplemented 10% FBS, 1% antibiotic-antimycotic (Biosharp, CHN) and 2 ng/mL FGF-2 (Sigma-Aldrich, USA). MSCs were seeded at an initial concentration of 5×10^6 cells/mL and maintained at 37°C in a humidified atmosphere containing 5% CO_2. The medium of MSCs was replaced every three days and cells were subcultured after reaching 70–80% confluence. Prior to encapsulation, MSCs were detached using trypsin, collected by centrifugation, and resuspended at a final density of 1×10^7 cells/mL. To reduce cell sedimentation and obtain buoyancy matching, the density of the cell-containing medium was adjusted to 1.06 g/mL by adding 16% (v/v) OptiPrep (Sigma-Aldrich, USA).

2.3 Cell Viability Determination by MTT Assay

HepG2 cells were seeded in 96-well plates at a density of 1×10^4 cells/well and incubated at 37°C with 5% CO_2 for 24 h to reach 70–80% confluence. The Schisandra extract was then applied to the wells at final concentrations ranging from 1.8 to 10 μM. Notably, the concentration of the extract was standardized based on the content of deoxyschisandrin, as quantified by GC-MS. After a 24 h treatment, 50 μL of MTT stock solution (1 mg/mL in PBS) was added to each well and incubated for 4 h. Subsequently, the supernatants were carefully aspirated, and the resulting formazan crystals were dissolved in 150 μL of DMSO for 10 min

with gentle agitation. The absorbance was measured at 490 nm using a microplate reader. All experiments were performed in triplicate, and cell viability was expressed as a percentage relative to the untreated control group.

2.4 Microfluidic Chip Fabrication

Microfluidic flow-focusing devices were prepared using conventional soft lithography methods. Polydimethylsiloxane (PDMS, Sylgard 184, Dow Corning, USA) was poured onto SU-8 photoresist patterned silicon master wafers for droplet generation devices, vacuumed until no visible bubbles remained, and cured overnight at 70°C. For the droplet-generating region, the aqueous-phase and oil-phase channels had cross-sectional dimensions of 50 × 80 μm and 50 × 30 μm (height × width), respectively. PDMS slabs were subsequently cleaned with ethanol, dried with nitrogen, and bonded to glass slides following oxygen plasma treatment. To improve bonding stability, the assembled PDMS devices were maintained at 70°C prior to use.

2.5 Fabrication of SLs-MSC-Laden Microgels

Before droplet generation, the inner surfaces of the microfluidic channels were modified with Aquapel (PPG Industries, USA) to create a hydrophobic environment favorable for stable emulsion formation. The hydrogel precursor was prepared by combining 20 wt% PEGNB (MW 20,000), 20 mM dithiol linker (MW 1,500; Sigma-Aldrich, USA), and 0.2 wt% LAP. To facilitate subsequent measurement of hydrogel microsphere size, 0.01 wt% thiolated Rhodamine B was incorporated into the precursor formulation and covalently integrated into the hydrogel network during polymerization. The SLs solution was added to the prepared precursor, and the mixture was vortexed for 60 s to achieve uniform dispersion. This solution was then injected into the microfluidic channels via a syringe pump, alongside MSC suspension at the same flow rate for on-chip mixing, resulting in a final concentration of 10 wt% PEGNB, 10 mM dithiol linker, 0.1 wt% LAP and 1.8 μg/mL SLs solution, and 1×10^7 cells/mL MSCs. For droplet generation, the aqueous phase and oil phase were introduced at flow rates of 1 μL/min and 5 μL/min, respectively. The resulting droplets were collected into centrifuge tubes and polymerized by UV irradiation. The height of the UV device was fixed. After UV exposure at an intensity of 100 mW/cm^2 for 20 s, the SLs-MSC-laden microgels were transferred and incubated within an ultralow attachment 6-well plate in the incubator.

2.6 Fabrication of Bulk Hydrogels

To encapsulate the LPS-induced HepG2 cells together with the SLs-MSC-laden microgels within hydrogels, HepG2 cells were cultured in serum-free DMEM for 4 h and then stimulated with LPS (1 μg/mL). After incubating for 24 h, the HepG2 cells were suspended at a cell density of 1×10^7 cells/mL. HepG2 cell suspension was mixed with SLs-MSC-laden microgels at a volume ratio of 1:4. Within a syringe (1 mL) with the needle trimmed off, the mixture was then mixed with PEGNB precursor solution to a final volume of 200 μL, resulting in the final concentration of 10 wt% PEGNB, 10 mM dithiol linker, 0.1 wt% LAP. After UV exposure at an intensity of 100 mW/cm^2 for 20 s, the hydrogel was removed from the syringe and incubated within an ultralow attachment 6-well plate in the incubator.

2.7 In Vitro Drug Release Study

The *in vitro* release of SLs from microgels was evaluated using deoxyschisandrin as a marker compound. Quantification was initially established using GC-MS. For routine analysis of PBS-based release samples with frequent sampling over an extended period, an HPLC-UV method was adopted due to its higher throughput, operational simplicity, and robust performance in aqueous matrices. Quantification was performed on

an HPLC system (Agilent 1100 series, USA) equipped with a UV detector and a Dikma Diamonsil C18 (2) column (250 mm × 4.6 mm, 5 μm; Dikma, China). A mixture of methanol-water (7:3, v/v) served as mobile phase. Sample solution was injected at a volume of 10 μL. Elution was performed in an isocratic mode at a flow-rate 1 mL/min and the detection at 254 nm. To quantify the amount of deoxyschisandrin encapsulated in the microgels, a standard calibration curve was created. The total loading amount of deoxyschisandrin for release was determined by the initial marker concentration and the volume fraction of the SLs stock solution introduced into the gel-forming precursor during microgel preparation. For the release assay, SLs-laden microgels were immersed in 5 mL of fresh PBS (pH = 7.4) and incubated at 37°C with gentle agitation. At predetermined time points (0, 1, 2, 3, 4, 5, 6, 9, 12, and 14 days), 1 mL of the release medium was withdrawn and immediately replaced with an equal volume of fresh PBS. The concentration of deoxyschisandrin in the collected samples was measured by HPLC. The cumulative release (%) of deoxyschisandrin was calculated relative to the initial loading amount, with correction for the withdrawn and replaced medium at each sampling time point. All experiments were performed in triplicate.

2.8 Cell Viability Assay

The viability of encapsulated MSCs was evaluated over a 14-day period using a membrane integrity-based LIVE/DEAD Viability Kit (Life Technologies, USA), in which live cells are labeled green and dead cells are stained red. Fluorescence micrographs were captured with an inverted fluorescence microscope (IX-71, Olympus, USA). For each time point, cell viability was calculated in ImageJ by quantifying 100 MSC-laden microgel particles.

2.9 Gene Expression Analysis

To evaluate the anti-inflammatory effects of different treatments, the LPS-induced HepG2 cells were encapsulated within the fabricated PEGNB hydrogels and co-encapsulated with different microgels, including SLs-laden microgels, MSC-laden microgels, and SLs-MSC-laden microgels. The sequences of the primers were shown in Table 1. For MSC gene expression analysis, total RNA was extracted from the following MSC samples: (i) LPS-induced MSCs cultured in monolayer, (ii) LPS-induced MSC-laden microgels, and (iii) LPS-induced SLs-MSC-laden microgels. Microgel samples were mechanically homogenized (crushed) in Trizol reagent (Biosharp, CHN) prior to RNA isolation. For HepG2 gene expression analysis, total RNA was extracted from the following HepG2 samples: (i) monolayer-cultured HepG2 cells (control), (ii) LPS-induced HepG2 cells cultured in monolayer, (iii) LPS-induced HepG2 cells encapsulated in bulk PEGNB hydrogels and co-encapsulated with MSC-laden microgels, (iv) LPS-induced HepG2 cells encapsulated in bulk PEGNB hydrogels and co-encapsulated with SLs-laden microgels, and (v) LPS-induced HepG2 cells encapsulated in bulk PEGNB hydrogels and co-encapsulated with SLs-MSC-laden microgels. All hydrogel constructs were mechanically homogenized (crushed) in Trizol reagent (Biosharp, CHN) prior to RNA isolation. HepG2 cells (human) and MSCs (mouse) were analyzed using species-specific qPCR primers to distinguish cell-type-derived transcripts in the homogenized co-encapsulated samples. Total RNA was isolated and purified using Total RNA Isolation Reagent (Biosharp, China) according to the supplier's instructions. Complementary DNA (cDNA) was then synthesized by reverse transcription with the First Strand cDNA Synthesis Kit (Biosharp, China). Quantitative polymerase chain reaction (qPCR) was performed with Universal SYBR qPCR Master Mix (Biosharp, CHN) following the manufacturer's protocol to measure the relative gene expression of selected genes, including TNF-α, IL-6, IL-10 and transforming growth factor-beta 1 (TGF-β1). For HepG2 cells, TNF-α and IL-6 expression levels were normalized against GAPDH, whereas β-actin was used as the internal reference for IL-10 and TGF-β1 expression in MSCs. Changes in gene expression

between the experimental and control groups were calculated using the comparative C_T method. The primer sequences used for qPCR are listed below:

Table 1: Forward and reverse primers used in this study.

Species	Gene	Forward Primer (5′-3′)	Reverse Primer (5′-3′)
Human	TNF-α	CCTCTCTCTAATCAGCCCTCTG	GAGGACCTGGGAGTAGATGAG
	IL-6	GGCACTGGCAGAAAACAACC	GCAAGTCTCCTCATTGAATCC
	GAPDH	AGGTCGGTGTGAACGGATTTG	TGTAGACCATGTAGTTGAGGTCA
Mouse	IL-10	AAGGCAGTGGAGCAGGTGAA	CCAGCAGACTCAATACACAC
	TGF-β1	TGAACCAAGGAGACGGAATACAGG	GCCATGAGGAGCAGGAAGGG
	β-actin	GATTACTGCTCTGGCTCCTA	ATCGTACTCCTGCTTGCTGA

2.10 Statistical Analysis

All data are shown as the mean ± SD (standard deviation). Statistical tests were performed using an unpaired *T* test and two-way ANOVA with GraphPad PRISM 6 software. Experiments were performed using three independent biological replicates, with technical triplicates for each measurement.

3 Results and Discussion

3.1 Extraction and Optimization of Schisandra Lignan Extract

GC-MS analysis of the Schisandra chinensis extract confirmed the presence of key bioactive lignans, primarily deoxyschisandrin and schisandrin (Fig. 1 and Table 2). Quantification was performed using the external standard method based on calibration curves established with commercial deoxyschisandrin standard (purity ≥ 98%, Macklin, China) and schisandrin standard (purity ≥ 97%, Macklin, China). Quantitative analysis revealed that the 1.5 h ethanol reflux following pre-washing yielded 0.83 mg/g of deoxyschisandrin and 2.51 mg/g of schisandrin from the raw powder. To optimize the extraction efficiency, different reflux durations (30, 60, and 90 min) were evaluated. As illustrated in Fig. 2, the yields of both bioactive lignans reached their peak at 90 min. Specifically, for deoxyschisandrin, the yield at 90 min was significantly higher than that at 60 min ($p < 0.01$). While the yield of schisandrin reached a plateau after 60 min with no significant further increase observed at 90 min ($p > 0.05$), the 90 min duration ensured the maximum recovery for both compounds. 90 min was selected as the optimal extraction time for subsequent pharmacological studies. Furthermore, the extract demonstrated excellent stability during storage at −20°C for 24 h, with no detectable degradation or alterations in lignan profiles. These findings validate that the optimized extraction process provides a stable and reliable source of lignans for subsequent pharmacological investigations.

Table 2: Bioactive compounds identified in the extract of Schisandra Lignan by GC-MS.

No.	RT	Name of the Compound	Molecular Formula	MW	Peak Area %
1.	31.662	deoxyschizandrin	$C_{24}H_{32}O_6$	416	5.51
2.	32.446	schisandrin	$C_{24}H_{32}O_7$	432	1.51

3.2 MTT Assay for Cytotoxicity Evaluation

The biocompatibility of SLs is a prerequisite for their therapeutic application. The cytotoxicity of SLs toward HepG2 cells was evaluated using the MTT assay (Fig. 3). Compared with the control (0 μM), SLs at 1.8 μM significantly increased the MTT signal to ~150% ($^*p < 0.05$), which indicate enhanced cellular metabolic

activity. No significant change in cell viability was observed at 3.2 and 5.6 μM (ns, $p > 0.05$). In contrast, cell viability decreased significantly at 7.5 μM (~55%, $^{*}p < 0.05$) and further declined at 10 μM (~25–30%, $^{**}p < 0.01$). Accordingly, the IC_{50} was estimated to fall between 7.5 and 10 μM, and concentrations ≤ 5.6 μM were selected as a non-cytotoxic working range for subsequent *in vitro* studies.

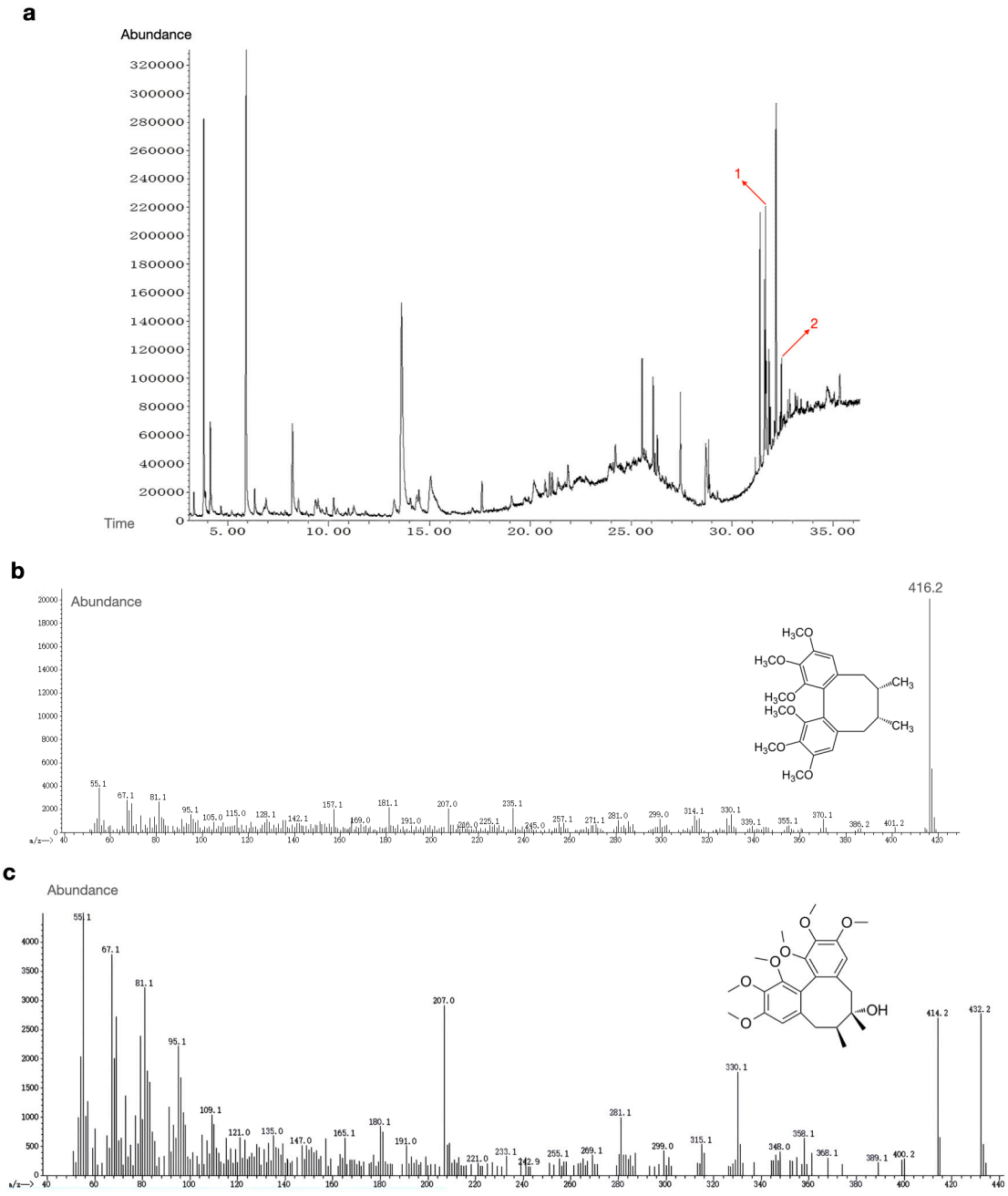

Figure 1: GC-MS characterization of the ethanolic lignan extract from Schisandra chinensis. (**a**) Total ion chromatogram (TIC) of the extract. Peaks: 1, deoxyschisandrin; 2, schisandrin. (**b**) EI mass spectrum and chemical structure of deoxyschisandrin. (**c**) EI mass spectrum and chemical structure of schisandrin.

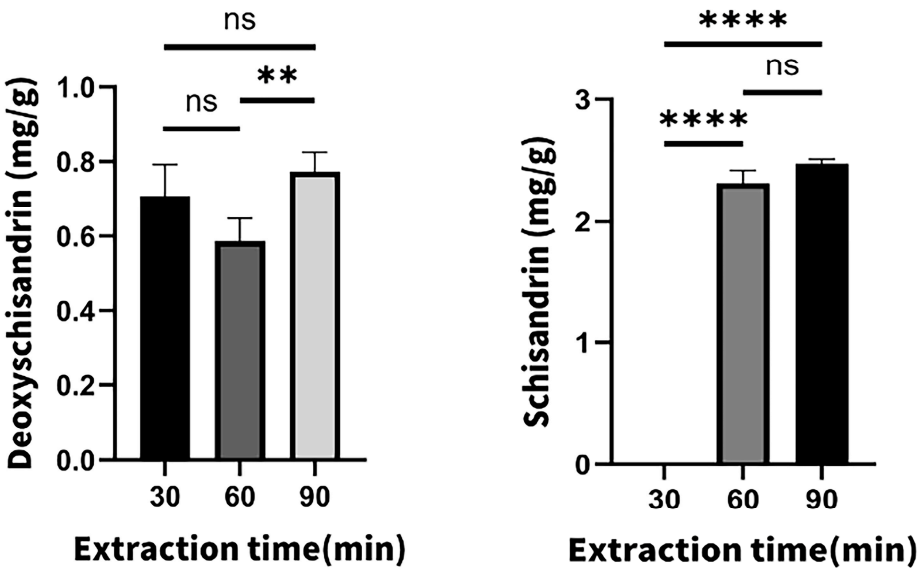

Figure 2: Yields (mg g^{-1} dry powder) of deoxyschisandrin and schisandrin extracted from Schisandra chinensis powder at different extraction times. $^{****}p < 0.0001$, $^{**}p < 0.01$, n.s.—non-significant.

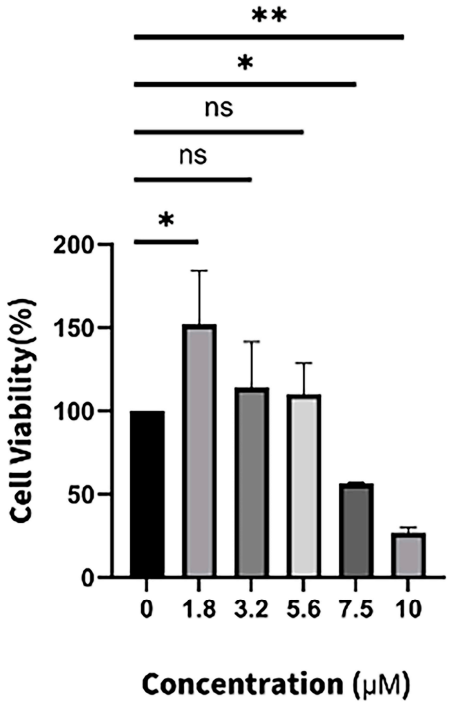

Figure 3: The effect of different concentrations of SLs (1.8, 3.2, 5.6, 7.5, 10 μM) for 24 h on HepG2 cells was investigated by MTT assay. $^{**}p < 0.01$, $^{*}p < 0.05$, n.s.—non-significant.

3.3 Microfluidic Fabrication and Sustained Release Profiles of PEGNB Microgels

Relatively uniform PEGNB microgels were generated using the microfluidic flow-focusing device to encapsulate both MSCs and SLs. Based on our established PEGNB microgel platform, aqueous and oil phase flow rates were controlled to generate PEGNB microgels with diameters ranging from 130 to 170 μm and high monodispersity. Microgel diameters were measured from fluorescence microscopy images using ImageJ, with 50 microgels analyzed per group (Fig. 4a). The morphology of PEGNB gels was characterized

by SEM in our previous study [33]. The optimized flow conditions ensured homogeneous droplet formation and effective encapsulation. The encapsulation of MSCs at a concentration of 1×10^7 cells/mL was achieved without compromising cell viability as confirmed by live/dead staining and quantitative viability analysis (Fig. 4b,c). After encapsulation, the cells exhibited high viability as previous research described. SLs were incorporated into the microgels by mixing the Schisandra lignans solution with the microgel precursor at a final concentration of 1.8 μg/mL (approximately 4.3 μM). Notably, the total amount of deoxyschisandrin loaded for release was determined by the volume fraction of the SLs stock solution incorporated into the gel-forming precursor during microgel preparation. The *in vitro* drug release profile was assessed by quantifying the SLs concentrations at predetermined time points over a 14-day period. The results demonstrated that the microgels released SLs in a controlled and sustained manner, reaching a cumulative release of approximately 82.31 ± 4.35% by Day 14 (Fig. 4d). This sustained delivery profile is highly significant for hepatitis therapy, as prolonged drug availability is essential for enhancing the anti-inflammatory effects of SLs. The generated microgels were encapsulated with the LPS-induced HepG2 cells within PEGNB hydrogels. The microenvironment offered by HepG2 cells mimicked the hepatitis microenvironment, thereby this setup enabled the evaluation of MSCs and SLs combined therapeutic efficacy under inflammation conditions that closely resemble *in vivo*.

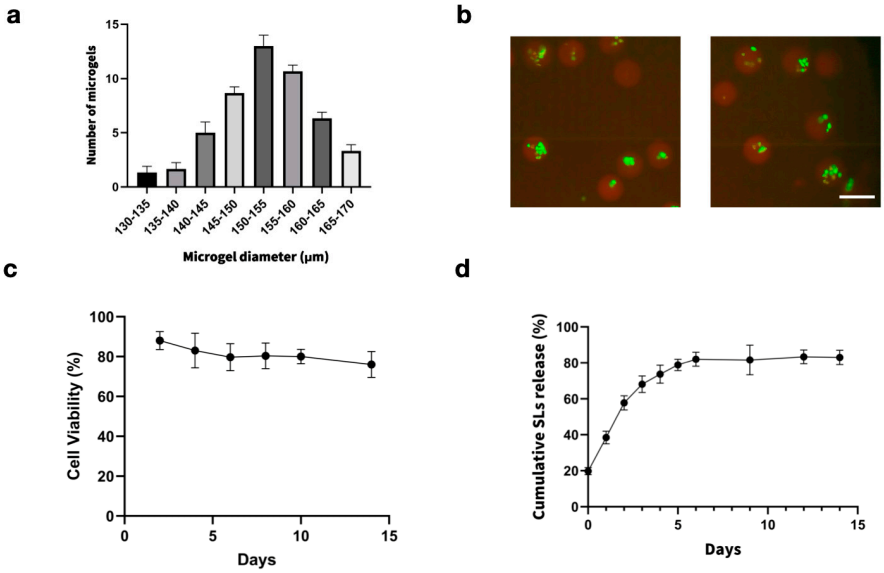

Figure 4: Biocompatibility and sustained release properties of the MSCs/SLs co-encapsulated PEGNB microgels. (**a**) Size distribution of PEGNB microgels fabricated at a gel:oil flow rate ratio of 2:10. Diameters were measured from fluorescence microscopy images using ImageJ. A total of 50 microgels were analyzed. (**b**) Representative fluorescence images of encapsulated MSCs (green indicates live cells, red indicates dead cells). Scale bar = 100 μm. (**c**) Quantitative analysis of MSC viability over 14 days after encapsulation. (**d**) Cumulative release profile of SLs from the microgels over 14 days, quantified using deoxyschisandrin as a marker compound. Data are shown as mean ± SD (n = 3).

3.4 Anti-Inflammatory Effects of SLs-MSC-Laden Microgels

The anti-inflammatory effects of SLs-MSC-laden microgels were evaluated by analyzing the expression of selected genes using qPCR. As shown in Fig. 5a, microencapsulation of MSCs under LPS stimulation markedly upregulated MSC-derived anti-inflammatory markers, including IL-10 and TGF-β1, compared with the LPS group, indicating that the microgel microenvironment promotes an enhanced immunomodulatory

phenotype of MSCs. LPS-induced HepG2 cells were treated with SLs-laden, MSC-laden microgels and SLs-MSC-laden microgels. As shown in Fig. 5b, treatment with SLs-MSC-laden microgels resulted in a significant reduction in the expression of TNF-α and IL-6 compared with the LPS treatment group, and the reduction was further enhanced relative to the SLs group and MSCs group, indicating the combined anti-inflammatory effects of SLs and MSCs. Specifically, LPS stimulation robustly increased TNF-α and IL-6 expression in HepG2 compared with the control group, whereas co-encapsulation with MSC-laden microgels partially attenuated this induction, consistent with MSC-mediated paracrine suppression of inflammatory signaling. SLs-laden microgels also reduced TNF-α and IL-6 levels, suggesting a direct anti-inflammatory contribution from SLs. Notably, the SLs-MSC-laden microgels achieved the most pronounced downregulation, yielding the lowest TNF-α and IL-6 expression among all tested groups. Under the same LPS-induced inflammatory conditions, the expression of MSC-derived anti-inflammatory genes, IL-10 and TGF-β1, was consistently upregulated in the combined group. Our findings are consistent with previous PEGNB microgel-based MSC delivery studies, which reported favorable MSC viability and enhanced paracrine activity after microencapsulation [36]. Based on previous reports that PEG hydrogels are generally regarded as biologically inert blank slates and that non-degradable PEG systems can evoke minimal inflammatory responses [42,43], we inferred that PEGNB alone was unlikely to induce a marked immune response in our system.

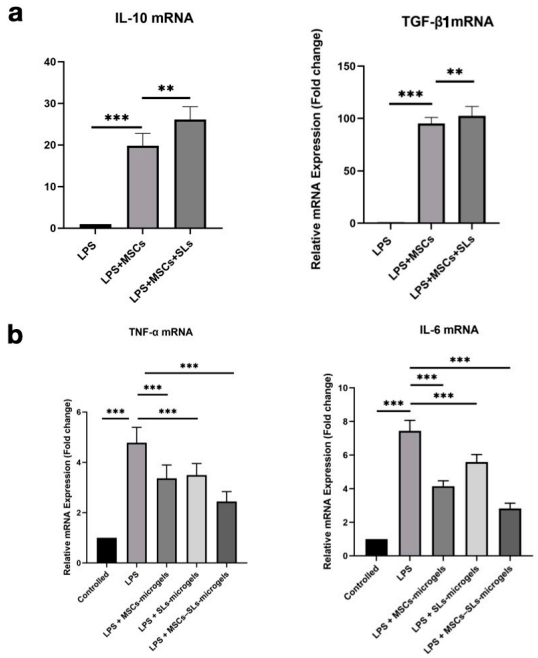

Figure 5: Synergistic immunomodulatory effects of the MSCs/SLs-laden microgel system. (**a**) Relative mRNA expression of anti-inflammatory markers (IL-10 and TGF-β1) under three conditions, the results are normalized to that of monolayer MSCs. (**b**) Relative mRNA expression of HepG2-derived pro-inflammatory cytokines (TNF-α and IL-6) across five groups.the results are normalized to that of monolayer HepG2. Data are expressed as mean ± SD (n = 5). $^{**}p < 0.01$, $^{***}p < 0.001$.

4 Conclusions

In this study, we fabricated SLs-MSC-laden microgels using a microfluidic flow-focusing device. The microgels exhibited sustained drug release, ensuring controlled delivery of SLs and MSC-derived cytokines. Through qPCR analysis, we demonstrated that the microgels significantly reduced the expression of pro-

inflammatory genes TNF-α and IL-6 in the LPS-induced HepG2 cells and promoted MSCs' paracrine activities. These findings highlight the potential of SLs-MSC-laden microgels as a promising therapeutic platform for modulating hepatic inflammation. This study provides a novel strategy for hepatitis-related inflammation by integrating natural bioactives, MSC immunomodulation, and PEGNB microgel-mediated localized delivery. However, the LPS-induced HepG2 model cannot fully represent the complexity of hepatic inflammation *in vivo*, particularly immune-cell interactions and systemic regulation. Future studies should focus on exploring the microgels' efficacy *in vivo* and assessing their long-term safety and potential for clinical translation.

Acknowledgement: Not applicable.

Funding Statement: This work was supported by the Liaoning Province Ph.D. Start-Up Program (2023BS-183), and the University of Science and Technology Liaoning Excellent Young Faculty Program (2023YQ09).

Author Contributions: The authors confirm contribution to the paper as follows: study conception and design: Xingdan Wang, Ni Ren; data collection: Xingdan Wang, Lei Yang, Yuheng Du, Linhao Zhu; analysis and interpretation of results: Xingdan Wang, Lei Yang, Renmeng Liu; draft manuscript preparation: Xingdan Wang, Lei Yang, Zhihuan Li, Xinyue Zhang; review: Renmeng Liu, Yuheng Du, Zhihuan Li, Xinyue Zhang, Linhao Zhu. All authors reviewed and approved the final version of the manuscript.

Availability of Data and Materials: Data will be made available on request.

Ethics Approval: Not applicable.

Conflicts of Interest: The authors declare no conflicts of interest.

References

1. Cao G, Jing W, Liu J, Liu M. The global trends and regional differences in incidence and mortality of hepatitis A from 1990 to 2019 and implications for its prevention. Hepatol Int. 2021;15(5):1068–82. [CrossRef].
2. Alberts CJ, Clifford GM, Georges D, Negro F, Lesi OA, Hutin YJ, et al. Worldwide prevalence of hepatitis B virus and hepatitis C virus among patients with cirrhosis at country, region, and global levels: A systematic review. Lancet Gastroenterol Hepatol. 2022;7(8):724–35. [CrossRef].
3. Abro AH, Abdou AM, Saleh AA, Ustadi AM, Hussaini HS. Hepatitis E: A common cause of acute viral hepatitis. J Pak Med Assoc. 2009;59(2):92–4.
4. Ginès P, Krag A, Abraldes JG, Solà E, Fabrellas N, Kamath PS. Liver cirrhosis. Lancet. 2021;398(10308):1359–76. [CrossRef].
5. Yuan H, Xu R, Li S, Zheng M, Tong Q, Xiang M, et al. The malignant transformation of viral hepatitis to hepatocellular carcinoma: Mechanisms and interventions. MedComm. 2025;6(3):e70121. [CrossRef].
6. McClune AC, Tong MJ. Chronic hepatitis B and hepatocellular carcinoma. Clin Liver Dis. 2010;14(3):461–76. [CrossRef].
7. Das M, Sabio G, Jiang F, Rincón M, Flavell RA, Davis RJ. Induction of hepatitis by JNK-mediated expression of TNF-α. Cell. 2009;136(2):249–60. [CrossRef].
8. Tiegs G, Horst AK. TNF in the liver: Targeting a central player in inflammation. Semin Immunopathol. 2022;44(4):445–59. [CrossRef].
9. Schuster S, Cabrera D, Arrese M, Feldstein AE. Triggering and resolution of inflammation in NASH. Nat Rev Gastroenterol Hepatol. 2018;15(6):349–64. [CrossRef].
10. Aggarwal BB. Signalling pathways of the TNF superfamily: A double-edged sword. Nat Rev Immunol. 2003;3(9):745–56. [CrossRef].
11. Elgazar AA, Selim NM, Abdel-Hamid NM, El-Magd MA, El Hefnawy HM. Isolates from *Alpinia officinarum* Hance attenuate LPS-induced inflammation in HepG2: Evidence from *in silico* and *in vitro* studies. Phytother Res. 2018;32(7):1273–88. [CrossRef].

12. Hegde S, Balasubramanian B, Paul R, Jayalakshmi M, Nizam A, Pappuswamy M, et al. Navigating green synthesized metal-based nanoparticles as anti-inflammatory agent—Comprehensive review. Int J Pharm. 2025;670:125105. [CrossRef].
13. Panossian A, Wikman G. Pharmacology of *Schisandra chinensis* Bail.: An overview of Russian research and uses in medicine. J Ethnopharmacol. 2008;118(2):183–212. [CrossRef].
14. Hu D, Han N, Yao X, Liu Z, Wang Y, Yang J, et al. Structure-activity relationship study of dibenzocyclooctadiene lignans isolated from *Schisandra chinensis* on lipopolysaccharide-induced microglia activation. Planta Med. 2014;80(8–9):671–5. [CrossRef].
15. Yan LS, Kang JY, Gu CY, Qiu XY, Li JJ, Cheng BC, et al. *Schisandra chinensis* lignans ameliorate hepatic inflammation and steatosis in methionine choline-deficient diet-fed mice by modulating the gut-liver axis. J Ethnopharmacol. 2025;348:119801. [CrossRef].
16. Guo LY, Hung TM, Bae KH, Shin EM, Zhou HY, Hong YN, et al. Anti-inflammatory effects of schisandrin isolated from the fruit of *Schisandra chinensis* Baill. Eur J Pharmacol. 2008;591(1–3):293–9. [CrossRef].
17. Luo G, Cheng BC, Zhao H, Fu XQ, Xie R, Zhang SF, et al. *Schisandra chinensis* lignans suppresses the production of inflammatory mediators regulated by NF-κB, AP-1, and IRF3 in lipopolysaccharide-stimulated RAW264.7 cells. Molecules. 2018;23(12):3319. [CrossRef].
18. Zhu L, Li B, Liu X, Huang G, Meng X. Isolation and purification of schisandrol A from the stems of *Schisandra chinensis* and cytotoxicity against human hepatocarcinoma cell lines. Pharmacogn Mag. 2015;11(41):131–5. [CrossRef].
19. Kamyab H, Khalili E, Khademi T, Yuzir A, Taheri MM, Rajendran S, et al. Advances in green synthesis of nanoparticles for biomedical applications: Antimicrobial, antiviral, and cancer therapies. Mater Today Sustain. 2026;33:101287. [CrossRef].
20. Liu P, Qian Y, Liu X, Zhu X, Zhang X, Lv Y, et al. Immunomodulatory role of mesenchymal stem cell therapy in liver fibrosis. Front Immunol. 2022;13:1096402. [CrossRef].
21. An R, Zhu Z, Chen Y, Guan W, Wang J, Ren H. MSCs suppress macrophage necroptosis and foster liver regeneration by modulating SP1/SK1 axis in treating acute severe autoimmune hepatitis. Adv Sci. 2025;12(12):2408974. [CrossRef].
22. Hu C, Wu Z, Li L. Mesenchymal stromal cells promote liver regeneration through regulation of immune cells. Int J Biol Sci. 2020;16(5):893–903. [CrossRef].
23. Weiss ARR, Dahlke MH. Immunomodulation by mesenchymal stem cells (MSCs): Mechanisms of action of living, apoptotic, and dead MSCs. Front Immunol. 2019;10:1191. [CrossRef].
24. Maacha S, Sidahmed H, Jacob S, Gentilcore G, Calzone R, Grivel JC, et al. Paracrine mechanisms of mesenchymal stromal cells in angiogenesis. Stem Cells Int. 2020;2020:4356359. [CrossRef].
25. Liu Y, Wang L, Kikuiri T, Akiyama K, Chen C, Xu X, et al. Mesenchymal stem cell-based tissue regeneration is governed by recipient T lymphocytes via IFN-γ and TNF-α. Nat Med. 2011;17(12):1594–601. [CrossRef].
26. Nauta AJ, Fibbe WE. Immunomodulatory properties of mesenchymal stromal cells. Blood. 2007;110(10):3499–506. [CrossRef].
27. Xiao K, He W, Guan W, Hou F, Yan P, Xu J, et al. Mesenchymal stem cells reverse EMT process through blocking the activation of NF-κB and Hedgehog pathways in LPS-induced acute lung injury. Cell Death Dis. 2020;11(10):863. [CrossRef].
28. Jiang Z, Jiang K, McBride R, Oakey JS. Comparative cytocompatibility of multiple candidate cell types to photoencapsulation in PEGNB/PEGDA macroscale or microscale hydrogels. Biomed Mater. 2018;13(6):065012. [CrossRef].
29. Kirkpatrick BE, Dhand AP, Hibbard LP, Jaeschke MW, Yendamuri T, Nelson BR, et al. Ultrafast-relaxing and photopolymerizable PEG hydrogels enable viscoelasticity-mediated cell remodeling in synthetic matrices. Matter. 2026;9(2):102524. [CrossRef].
30. Jiang Z, Xia B, McBride R, Oakey J. A microfluidic-based cell encapsulation platform to achieve high long-term cell viability in photopolymerized PEGNB hydrogel microspheres. J Mater Chem B. 2017;5(1):173–80. [CrossRef].
31. Mabry KM, Lawrence RL, Anseth KS. Dynamic stiffening of poly(ethylene glycol)-based hydrogels to direct valvular interstitial cell phenotype in a three-dimensional environment. Biomaterials. 2015;49:47–56. [CrossRef].

32. Kloxin AM, Kasko AM, Salinas CN, Anseth KS. Photodegradable hydrogels for dynamic tuning of physical and chemical properties. Science. 2009;324(5923):59–63. [CrossRef].
33. Jiang Z, Shaha R, McBride R, Jiang K, Tang M, Xu B, et al. Crosslinker length dictates step-growth hydrogel network formation dynamics and allows rapid on-chip photoencapsulation. Biofabrication. 2020;12(3):035006. [CrossRef].
34. Shaha R, Jiang Z, Frick CP, Oakey J. Cell-laden particulate-composite hydrogels with tunable mechanical properties constructed with gradient-interface hydrogel particles. ACS Appl Polym Mater. 2019;1(10):2571–6 [CrossRef].
35. Burdick JA, Anseth KS. Photoencapsulation of osteoblasts in injectable RGD-modified PEG hydrogels for bone tissue engineering. Biomaterials. 2002;23(22):4315–23. [CrossRef].
36. Si H, Chen Y, Jiang K, Ma K, Ramsey E, Oakey J, et al. Deterministic single-cell encapsulation in PEG norbornene microgels for promoting anti-inflammatory response and therapeutic delivery of mesenchymal stromal cells. Adv Healthc Mater. 2024;13(14):e2304386. [CrossRef].
37. Jiang Z, Lin FY, Jiang K, Nguyen H, Chang CY, Lin CC. Dissolvable microgel-templated macroporous hydrogels for controlled cell assembly. Biomater Adv. 2022;134:112712. [CrossRef].
38. Jiang Z, Jiang K, Si H, McBride R, Kisiday J, Oakey J. One step encapsulation of mesenchymal stromal cells in PEG norbornene microgels for therapeutic actions. ACS Biomater Sci Eng. 2023;9(11):6322–32. [CrossRef].
39. Dimmitt NH, Lin CC. Hydrolytic degradation of PEG-based thiol-norbornene hydrogels enables multi-modal controlled release. J Mater Chem B. 2025;13(42):13781–93. [CrossRef].
40. Qian C, Higashigaki T, Asoh TA, Uyama H. Anisotropic conductive hydrogels with high water content. ACS Appl Mater Interfaces. 2020;12(24):27518–25. [CrossRef].
41. Sivakumaran D, Maitland D, Oszustowicz T, Hoare T. Tuning drug release from smart microgel-hydrogel composites *via* cross-linking. J Colloid Interface Sci. 2013;392:422–30. [CrossRef].
42. Day JR, David A, Kim J, Farkash EA, Cascalho M, Milašinović N, et al. The impact of functional groups of poly(ethylene glycol) macromers on the physical properties of photo-polymerized hydrogels and the local inflammatory response in the host. Acta Biomater. 2018;67:42–52. [CrossRef].
43. Isaac AH, Recalde Phillips SY, Ruben E, Estes M, Rajavel V, Baig T, et al. Impact of PEG sensitization on the efficacy of PEG hydrogel-mediated tissue engineering. Nat Commun. 2024;15(1):3283. [CrossRef].